Sequential infiltration analysis of infiltration curves measured with disc infiltrometer in layered soils

D Moret-Fernández, B Latorre, L Lassabatere, S Di Prima, M Castellini, D Yilmaz, Rafaël Angulo-Jaramillo

When citing, please refer to the published version:

Moret-Fernandez, D., Latorre, B., Lassabatère, L., Di Prima, S., Castellini, M., Yilmaz, D., Angulo-Jaramillo, R., 2021. Sequential infiltration analysis of infiltration curves measured with disc infiltrometer in layered soils. Journal of hydrology, 600: 126542. https://doi.org/10.1016/j.jhydrol.2021.126542

Sequential infiltration analysis of infiltration curves measured with disc infiltrometer in layered soils

by

Moret-Fernández, D. [1,2*], Latorre, B.[1], Lassabatere, L.[3], Di Prima, S[4]., Castellini, M.[5], Yilmaz, D.[6], Angulo-Jaramilo, R.[3]

[1] Departamento de Suelo y Agua, Estación Experimental de Aula Dei, Consejo Superior de Investigaciones Científicas (CSIC), PO Box 13034, 50080 Zaragoza, Spain
[2] Instituto Pirenaico de Ecología (CSIC), Av. Montañana 1005, P.O. Box 13.034, 50080 Zaragoza, Spain
[3] Univ Lyon, Université Claude Bernard Lyon 1, CNRS, ENTPE, UMR5023 LEHNA, F-69518, Vaulx-en-Velin, France
[4] Department of Agricultural Sciences, University of Sassari, Viale Italia, 39, 07100 Sassari, Italy
[5] Council for Agricultural Research and Economics-Research Center for Agriculture and Environment (CREA-AA); mirko.castellini@crea.gov.it
[6] Munzur University, Engineering Faculty, Civil Engineering Department, 62000 Tunceli, Turkey

* Corresponding author. E-mail: david@eead.csic.es Tel.: (+34) 976 71 61 40

Sequential infiltration analysis of infiltration curves measured with disc infiltrometer in layered soils

Moret-Fernández, D. [1,2*], Latorre, B.[1], Lassabatere[3], L., Di Prima, S[4]., Castellini, M.[5], Yilmaz, D.[6], Angulo-Jaramilo[3], R.

[1] Departamento de Suelo y Agua, Estación Experimental de Aula Dei, Consejo Superior de Investigaciones Científicas (CSIC), PO Box 13034, 50080 Zaragoza, Spain

[2] Instituto Pirenaico de Ecología (CSIC), Av. Montañana 1005, P.O. Box 13.034, 50080 Zaragoza, Spain

[3] Univ Lyon, Université Claude Bernard Lyon 1, CNRS, ENTPE, UMR5023 LEHNA, F-69518, Vaulx-en-Velin, France

[4] Department of Agricultural Sciences, University of Sassari, Viale Italia, 39, 07100 Sassari, Italy

[5] Council for Agricultural Research and Economics-Research Center for Agriculture and Environment (CREA-AA); mirko.castellini@crea.gov.it

[6] Munzur University, Engineering Faculty, Civil Engineering Department, 62000 Tunceli, Turkey

* Corresponding author. E-mail: david@eead.csic.es Tel.: (+34) 976 71 61 40

Abstract

The soil sorptivity, S, and saturated hydraulic conductivity, K_s, can be estimated from the inverse analysis of a cumulative infiltration curve using the quasi-exact implicit (QEI) formulation or its corresponding 4-Terms (4T) approximation. Although these models consider the soil as homogeneous media, there is no information about how heterogeneous profiles can affect the inferred soil properties. This work analyzes the influence of layered soils on K_s and S estimates using QEI and 4T models, and designs a new procedure for treating infiltration curves measured on layered soil profiles. The Sequential Infiltration Analysis (SIA) method considers a sequence of increasing time series from the cumulative infiltration data to estimate K_s and S, and its corresponding RMSE as a function of the number of samples used. A procedure to estimate the thickness of the upper uniform soil layer from the estimated wetting front advance (WFA) is also reported. The SIA method was applied on: (i) synthetic homogeneous profiles of loam soil and six layered profiles involving a 1, 2 and 3 cm thickness loam layer over silty or sandy loam soils, respectively, (ii) stratified laboratory soil columns, and (iii) 20 experimental infiltrations performed in a semiarid region of North-Eastern Spain. Similar results were found between QEI and 4T models for all cases. Erroneous estimates of K_s and S were observed when the total infiltration time series was considered for the analysis, regardless of the presence of soil layering. In opposite, estimates improved when the SIA method was applied to the layered systems. The SIA method exploits the fact that the RMSE increases when the wetting front reaches the interface between the soil layers. Such increase allows: (i) detection of the soil heterogeneity, (ii) determination of the infiltration time, t_o, required for the wetting front to reach the lower layer, and, (iii) accurate estimates of the upper layer K_s and S along with its thickness. Laboratory experiments on layered soils and field measurements demonstrated that the SIA method could be satisfactorily applied on different curves with contrasting shapes and magnitudes. Although soil layering encountered on most

field samplings restricted the treatment of the observed infiltrations to short-medium times, the SIA method allowed robust estimates of K_s and S. These results indicate that the proposed method is a promising tool for characterizing the hydraulic properties of layered and heterogeneous soil profiles.

Keywords: Sorptivity; Hydraulic conductivity; Infiltration; Heterogeneous soil profiles

1. INTRODUCTION

Measurements of the soil surface hydraulic properties is crucial to solve many hydrological engineering and environmental issues linked to soil water storage and transport in the vadose zone. The tension disc infiltrometer (Perroux and White, 1988) has become a popular infiltration method because of the portable and its easy in-situ applicability (Angulo-Jaramillo et al., 2000). This instrument consists of a disc base attached to a water-supply reservoir and a bubbling tower to impose a negative pressure head (h) at the disc base (Perroux and White, 1988). The soil hydraulic properties, sorptivity (S) and hydraulic conductivity (K_s), are commonly calculated from the cumulative water-infiltration curve measured with the disc infiltrometer. To this end, methods based on the transient state data analysis can be employed. The main advantage of the transient methods, compared to water steady-state based procedures (Ankeny et al., 1991; Lassabatere et al., 2006), is that they allow shorter experiments, which involves smaller sampled soil volumes, and hence a more homogeneous soil and initial water content profile (Angulo-Jaramillo et al., 2000).

Among the different water transient models, the quasi-exact implicit (QEI) analytical formulation of Haverkamp et al. (1994) has become one of the most popular methods to

estimate the soil hydraulic properties (e.g., Lassabatere et al., 2009; Latorre et al., 2015, Fernandez-Galvez et al., 2019). The Haverkamp et al. (1994) model was extended to 3D disc infiltrometer measurements by Smettem et al. (1994) involving the following input parameters: K_s, S, the radius of the disc, r_d, the β and γ constants, and the initial and final volumetric water contents, θ_i and θ_s (Haverkamp et al., 1994; Smettem et al., 1994). The β shape parameter is related to the soil diffusivity, $D(\theta)$, and the soil hydraulic conductivity functions. The constant γ is related to the effect of the disk radius and gravity as well as the approximate estimation of sorptivity (Haverkamp et al., 1994, Smettem et al., 1994). Under regular conditions, a constant β and γ values of 0.6 and 0.75, respectively, are employed (Angulo-Jaramillo et al., 2019; Lassabatere et al. 2009; Latorre et al., 2018, Moret-Fernández et al., 2020). In order to simplify the mathematics reducing the number of input variables, Lassabatere et al. (2006) proposed packing $\Delta\theta$, r_d and γ into the $A = \frac{\gamma}{r_d(\theta_s - \theta_i)}$ term.

Given that direct formulations are more convenient than complex implicit equations, Haverkamp et al. (1994) proposed the simplified two-Terms (2T) approximation for their quasi-exact implicit (QEI) formulation. However, such an approximation remains valid only for short to intermediate infiltration times. Although this simplified model has been largely employed for characterizing soils (Vandervaere et al., 2000; Lassabatere et al., 2006; Moret-Fernández et al., 2013), its reduced temporal validity makes its use uncertain. To solve this limitation, Latorre et al. (2105) determined the soil hydraulic properties form the inverse analysis of the QEI model, instead of using approximations like in BEST methods (Lassabatere et al., 2006, Yilmaz et al., 2010, and Bagarello et al., 2014). On their track, Fernandez-Galvez et al. (2019) compute a new version of BEST that makes use of the QEI formulation. However, such formulation is implicit and could lead to numerical indetermination while slowing down the inversion procedure. Given those difficulties, Moret-Fernández et al. (2020) suggested estimating K_s and S using the three-Terms (3T) and four-

Terms (4T) approximations of the QEI formulation. These expansions are more accurate than the 2T, since they incorporate more terms, and thus remain valid over larger time intervals. Besides, the 4T model presents four degrees of freedom and thus the potential to estimate the four input variables: K_s, S, γ and β. However, Moret-Fernández et al. (2020) demonstrated that the inversion was affected by equifinality and non-uniqueness due to the small contribution of the fourth term to the bulk infiltration. Consequently, constant $A=\frac{\gamma}{r_d(\theta_s-\theta_i)}$ and β values are required in the inverse analysis of experimental infiltration curves measured with contact sand layer. As a corollary, because of γ and β values are strongly linked, unrealistic hydraulic properties values could be obtained.

Most models developed for water infiltration consider isotropic and homogeneous porous media. This means that soil hydraulic properties and initial water content are considered uniform in all directions. However, soil heterogeneity in the field is more the rule than the exception and this may strongly impact cumulative infiltrations (Iovino et al., 2017; Lassabatere et al., 2010; Lassabatere et al., 2014; Angulo-Jaramillo et al., 2019). For instance, double-slope infiltration curves may be obtained in case of hydrophobicity (Lassabatere et al., 2019) or infiltration curves with extra-concavity may be obtained due to soil sealing and the concomitancy of several layers (Di Prima et al., 2018). In these cases, the application of models based on soil uniformity can result in erroneous estimates of the soil hydraulic properties (Angulo-Jaramillo et al., 2019).

Given the scarce information on the application of inverting methods developed for uniform soils to non-uniform and layered soils, the objective of this work is to study the influence of layered profiles on K_s and S estimates obtained by fitting QEI, or its approximate expansions, to infiltration data. The second objective is the development of a procedure for an appropriate characterization of the soil hydraulic properties of the upper soil layer and to approximate its

thickness. To this end, both the QEI and 4T models were fitted to infiltration curves obtained (experimentally or numerically) in homogenous and layered soil profiles. The procedure implements a sequential analysis of the infiltration data series by fitting the model to an increasing number of samples and reporting the evolution of the quality of the fit or the RMSE. The best fit, characterized by the minimum RMSE, identifies the values of K_s and S from the upper layer, and provides the optimum infiltration time from which the thickness of the upper layer is also estimated. The new method, referred to as SIA for Sequential Infiltration Analysis, was validated using numerically generated data, laboratory experiments with homogeneous and layered soil profiles, and also real field data.

2. THEORY

2.1. Cumulative infiltration curve equations

The 3D cumulative infiltration, I_{3D}, model (QEI) for disc infiltrometer measurements corresponding to a zero water pressure head imposed at the soil surface (i.e., saturated conditions) can be described as follows (Haverkamp et al., 1994; Smettem et al. 1994):

$$I_{3D} = I_{1D} + A\,t \tag{1a}$$

$$A = \frac{\gamma S^2}{r_d(\theta_s - \theta_i)} \tag{1b}$$

where t is time (T), r_d is the radius of the disc (L), S is the sorptivity (L $T^{-0.5}$), and γ is a proportionality constant that accounts for the correction of the wetting front shape (Smettem et al., 1994). The A parameter, as originally defined by Lassabatere et al. (2006), quantifies the capillarity-driven lateral water flux (Lassabatere et al., 2006); and I_{1D}denotes the 1D

cumulative infiltration curve that can be modeled using the QEI formulation developed by Haverkamp et al. (1994):

$$\frac{2(K_s-K_i)^2}{S^2}t = \frac{2}{1-\beta}\frac{(K_s-K_i)(I_{1D}-K_i t)}{S^2} - \frac{1}{1-\beta}ln\left[\frac{1}{\beta}exp(2\beta(K_s-K_i)(I_{1D}-K_i t)/S^2) + \frac{\beta-1}{\beta}\right] \quad (2)$$

where K_s and K_i (L T^{-1}) are the hydraulic conductivity values corresponding to saturation, θ_s, and initial, θ_i, volumetric water content (L^3 L^{-3}), respectively, and β is the integral shape parameter. For regular working conditions, β varies between 0.6 and 1.7 (Lassabatere et al., 2009) and γ between 0.6 and 0.8 (Haverkamp et al., 1994).

The cumulative 3D infiltration curve can be also approximated with power series in $t^{1/2}$ (Fig. 1) as proposed by Haverkmap et al. (1994):

$$I_{3D}(t) = c_1 t^{\frac{1}{2}} + c_2 t + c_3 t^{\frac{3}{2}} + c_4 t^2 + c_5 t^{\frac{5}{2}} + \cdots \quad (3)$$

where c_i (L $T^{-i/2}$) are coefficients that depend on the soil hydraulic properties and the initial conditions. The application of Taylor series to the 3D QEI up to fourth order in powers of $t^{1/2}$ results in the following 4T approximation (Moret-Fernández et al., 2020):

$$I_{3D\_4T}(t) = St^{\frac{1}{2}} + \left(\frac{2-\beta}{3}K_s + AS^2\right)t + \frac{K_s^2}{9S}(\beta^2-\beta+1)t^{\frac{3}{2}} + 2(\beta-2)(\beta 1)\frac{(1-2\beta)}{135}\frac{K_s^3}{S^2}t^2 \quad (4)$$

Given that we have four unknown parameters (S, K_s, β and A), on one hand, and that four coefficients $(c_i)_{i\in\{1..4\}}$ are involved in the 4T approximate expansion, on the other, the inverse analysis can potentially determine the four unknowns. However, Moret-Fernández et al. (2020) demonstrated that the A and β parameters need to be fixed a priori for the case of water infiltration curve measured with the addition of a contact sand layer (such addition aims to improve the contact between the infiltration device and the soil). Given that inverting infiltration data for soil layered profile remains tricky, in the following, we defined a new method to analyze soilfor layered profiles.

162

163 *2.2. Sequential infiltration analysis (SIA) and soil surface layer thickness estimate*

164 Using both QEI and 4T models, the new procedure involves the analysis of a sequence of
165 increasing time series from the cumulative infiltration data. The SIA procedure estimates S
166 and K_s by fitting QEI or 4T to increasing time series and computes the RMSE as a function of
167 the number of samples. The optimal infiltration time, t_o, is identified by the minimum RMSE,
168 and its corresponding inversion provides the estimates of K_s and S. A total of 30 increasing
169 times ranged from 50s to the total available infiltration data were considered. The inverse
170 analysis with 4T (Eq. 7) was performed using a nonlinear (weighted) least-square method that
171 incorporates the Levenberg-Marquardt optimization algorithm. The procedure was
172 implemented into a function that returns a vector of (weighted) residuals whose sum square is
173 minimized (More, 1978; Bates and Watts, 1988; Bates and Chambers, 1992). To this end, the
174 R (R version 3.5.0. The R Foundation for Statistical Computing) software was employed. For
175 the QEI model, the global inverse analysis proposed by Latorre et al. (2015) was used. In this
176 case, S and K_s were estimated by minimizing an objective function that represents the
177 difference between the implicit model (Eq. 1) and the experimental cumulative infiltration
178 data. To this end, a brute-force search (Horst and Romeijn, 2002) was employed, enumerating
179 all possible candidates of the hydraulic parameters to a certain precision and selecting the best
180 result. In all cases, γ and β values were fixed at their recommended values, 0.75 and 0.6
181 respectively.

182 The thickness of the soil surface layer was defined as the position of the wetting front
183 advance (WFA) at time t_o. The position of the wetting front was calculated as (Lassabatere et
184 al., 2009):

185 $$WFA = \frac{I_{1D}(t_0)}{\theta_s - \theta_i} \quad (5)$$

where $I_{1D}(t_0)$ is calculated according to:

$$I_{1D}(t_0) = St_0^{\frac{1}{2}} + \left(\frac{2-\beta}{3}K_s\right)t_0 + \frac{K_s^2}{9S}(\beta^2 - \beta + 1)t_0^{\frac{3}{2}} + 2(\beta - 2)(\beta 1)\frac{(1-2\beta)}{135}\frac{K_s^3}{S^2}t_0^2 \quad (6)$$

using the previously optimized K_s, S and β = 0.6.

3. MATERIAL AND METHODS

3.1. Validation of SIA method with synthetic soils (numerically generated data)

The infiltration curves were simulated with HYDRUS-3D model (Šimunek et al., 1999). The van Genuchten (1980) model was selected for water retention curves and the Mualem's model (1976) for the unsaturated hydraulic conductivity defined for sandyloam, loam and silt soils (Carsel and Parrish, 1988) (Table 1). The soil volume was discretized as a cylinder (25 cm in radius and 25 cm depth), covering the axisymmetric plane with a 2D rectangular mesh of 100 x 900 cells. A disc infiltrometer of 10 cm in radius was represented by a fixed water pressure boundary with a value of 0 cm. A null pressure head was considered as bottom boundary. The initial soil water content corresponded to its residual water content. The synthetic data was computed for 2000 s, which corresponds to a regular experimental infiltration. In addition, we checked that this time was enough for the wetting front did not reach the lower layer. No contact sand layer was defined. More details about the cumulative infiltration curves generation can be found in Latorre et al. (2015). The simulations (Fig. 2) were performed on a homogeneous loam (L) soil and layered soil profiles consisting on a 1, 2, and 3 cm thickness loam soil followed by a sandy loam (L-SL) or silt (L-Si) synthetic soil, respectively. The θ_s and θ_i needed to estimate the soil hydraulic parameters are summarized in Table 1. The application of the SIA method leads to the results reported in Table 2 and that will be discussed in the Results section.

209

210 *3.2. Laboratory experiments*

211 Five laboratory infiltration experiments were conducted on different soil columns. The first
212 experiments consisted on three 15 cm depth and 30 cm diameter soil columns homogeneously
213 packed with sand (80 μm mean size particle), 2-mm sieved loam (28, 47, 25 and 1.2 % of
214 sand, silt, clay and organic carbon, respectively) and loam clay soils (20, 50, 30 and 2.0 % of
215 sand, silt, clay and organic carbon, respectively). The remaining experiments consisted on 30
216 cm diameter columns made with a 3 cm thickness upper layer of sand and loam soil, followed
217 by a 5 cm thickness clay loam layer (Fig. 3).

218 An infiltration curve was measured in each soil column using a 10 cm diameter Perroux
219 and White (1988) model tension disc infiltrometer. All the infiltration experiments are
220 considered to be 3D with no impact of the edges of the columns on the lateral expansion of
221 the infiltration bulb. All measurements were performed at soil saturation conditions at surface.
222 The water infiltration was monitored with ±35.2 cm differential pressure transducer
223 (Microswitch, Honeywell) at 1 s of time interval. Infiltration measurements continued
224 between 60 seconds and 1400 s. The initial and saturated soil water contents of the upper layer
225 were measured with the core method (Grossman and Reinsch, 2002). Similarly, as described
226 in the previous section, S, K_s and t_o were estimated with the SIA procedure using both 4T and
227 QEI models. A constant β and γ equal to 0.6 and 0.75 together with the actual disc radius and
228 the measured $\Delta\theta$ (Table 3) were employed. The RMSE and the *WFAs* were calculated as
229 described in the previous section. Negative K_s obtained from the inverse analysis were omitted
230 and fixed to 10^{-5} mm s^{-1}.

231

232 *3.3. Field measurements*

The infiltration measurements were performed on agro-pastoral fields located in the municipality of Mediana de Aragón (M1) (41º25′N, 0º44′W), in the Zaragoza province of Aragón (NE Spain). Average annual temperature and precipitation are 14.9 ºC and 350 mm yr^{-1}, respectively. The lithology in the area is mainly gypsum outcrops. Soils are Leptosols in the hills and Gypsisols in the flat-bottomed valleys (Navas, 1991). These are poorly developed soils, with a sandy loam to loam texture, high gypsum (between 680 and 940 g kg^{-1}) and low organic matter (between 9 to 48 g kg^{-1}) contents (Navas, 1991). Field infiltrations were performed on bare (R1) and soils with plants (R2) in fields with soil with low (L) and medium (M) grazing intensity.

A 50 mm in diameter and 50 mm in height undisturbed soil cores were sampled close to the infiltration points. The θ_s was measured by saturating the soil core, and subsequently drying it at 50 ºC during 48 h. The initial volumetric water content (θ_i) was measured with a DeltaT water content probe. One replication for θ_s and θ_i was performed per sampling site. A 10 cm diameter disc infiltrometer was employed. A thin layer (< 1 cm thick) of commercial sand (80–160 μm grain size) was placed between base disc and soil surface. The duration of the experiments varied between 500 and 1800 s, depending on the time needed to reach steady state infiltration conditions. A total of 20 cumulative infiltration curves were recorded. The influence of the contact sand layer (t_{sand}) on K_s and S estimates was removed using the procedure developed by Latorre et al. (2015). This consists of a layered flow model that assumes that water does not infiltrate into the soil until the sand layer is completely saturated. The sand effect is considered as a gap, in time and volume, before water infiltrates into the soil. The contact sand layer effect is removed by finding the sand infiltration time (and its corresponding water volume) and shifting the experimental data to the origin. The maximum infiltration time due to the sand wetting layer was fixed to 10 s. Consequently, for modeling

with the SIA method, we no longer considered the sandy layer. Only the soil layering, if any, is expected to have an effect on the cumulative infiltration curves.

The SIA method was then used, as described for the synthetic soils analysis, to provide S, K_s, t_o, RMSE and *WFA*. Both 4T and QEI models were considered for the application of the SIA method on the field measurements.

4. RESULTS AND DISCUSSION

4.1. Results for the synthetic soils (numerically generated data)

Except for the first infiltration times, S and K_s estimates for the homogeneous loam soil (L) using 4T were constant along the whole duration of the experiment (Fig. 4). The initial divergences could be attributed to the large tension difference at the beginning of the experiment, which changes from -10^{-3} to -10^{7} cm, and affects the numerical stability of the simulated cumulative infiltrations. Apart from this initial variation, the estimates remain constant along the experiment. This result indicates that, under homogeneous soil conditions, the considered infiltration time does not affect the predictions of the hydraulic parameters. Meanwhile, a slight decrease of RMSE was noticed with increasing time for the homogeneous synthetic loam column. This is due to the fact that the difference between the synthetic and simulated curves is divided by the total number of data-points. In addition, the RMSE change with increasing analyzed time resulted in an indicator of the soil heterogeneity, with no significant variations in the absence of soil layering. The RMSE represents the difference between the measured data and the theoretical curve, which is consistent with the hypothesis of a homogeneous soil. Consequently, the sudden increase of the RMSE is expected in the

279 presence of soil layering from the time when the infiltration bulb reaches the layers interface
280 and both curves (experimental and theoretical) begin to differ.

281 In heterogeneous or layered soil profiles, the RMSE increased at the time (t_o) when the
282 infiltration bulb reaches the lower soil layer (Fig. 4b). From time t_o, S and K_s started to deviate
283 from their theoretical values (Fig. 4c and d). Thus, these results indicate that the SIA method
284 using 4T detects the soil heterogeneity and identifies the maximum time (t_o) to be considered
285 for accurate estimations of S and K_s of the upper soil layer. In contrast, erroneous hydraulic
286 properties were reported when infiltration times larger than t_o are employed (Fig.4c and d).
287 For example, this is the case of the L_{1cm}+Si soil, where long time analysis resulted in smaller
288 K_s values. In this case, the significant decrease of K_s from t_o, should be attributed to the extra-
289 concavity of the infiltration curve promoted by the less permeable deeper soil layer (Di Prima
290 et al., 2018), which forces the model to reduce K_s to minimum threshold of 10^{-5} mm s^{-1} defined
291 in the optimization. For the L_{1cm}+SL synthetic soil, erroneous K_s estimates would be also
292 obtained if, for instance, long-time infiltration values were considered. In this respect, the
293 extra-convexity promoted by the more permeable deeper soil layer, makes K_s decreasing to
294 the minimum threshold of 10^{-5} mm s^{-1} just after t_o, to later stabilize K_s at a value close that
295 defined for SL (Table 1). These results indicate that K_s evolution from t_o contains valuable
296 information about the permeability of the deeper soil layer. In conclusion, these results
297 indicate that the infiltration time is an important factor to estimate the soil hydraulic properties
298 of heterogeneous soil profiles. The SIA method using the 4T model was an efficient tool to
299 detect soil homogeneity and to estimate S and K_s from the upper layer of heterogeneous soils.

300 Overall, good estimates of soil hydraulic properties were obtained when the SIA method,
301 using either 4T or QEI, was applied to the homogeneous synthetic loam soil (Table 2 versus
302 Table 1). In this case, the relative difference between theoretical and the optimized S and K_s

303 (K_s in log scale) were 0.45% and 3.17%, respectively. Similar results were reported by Latorre
304 et al. (2015) and Moret-Fernández et al. (2020). Except for the synthetic soil profiles with the
305 thinnest top soil layer (L_{1cm}+SL and L_{1cm}+Si), the S and K_s estimates with QEI and 4T also
306 agreed with their theoretical values (Table 2 versus Table 1). These results indicate that
307 accurate estimations of S and K_s require a minimum thickness of soil depth. The similarity of
308 the estimations using the QEI and 4T expansion in heterogeneous profiles (Table 2)
309 corroborates the 4T expansion was accurate enough for a proper estimation of the soil
310 hydraulic properties. This is an interesting result since the complexity of the Latorre et al.
311 (2015) procedure may restrict its use when the SIA method is applied on a large dataset of
312 infiltration measurements. This problem, however, vanishes using the 4T model, for which
313 the simpler equation allows fast and affordable analyses.

314 The numerical results also show that the prediction of the thickness of the upper soil layer is
315 quite accurate. Indeed, the calculated wetting front advance (*WFA*), were significantly
316 correlated to the real values of the top layer thickness ($y = 0.94x + 0.36$, $R^2 = 0.97$, $p < 0.0001$)
317 (Table 2). These results indicate that the thickness of the upper soil layer can be estimated
318 from the sequential analysis of the cumulative infiltration curve, using both QEI and 4T
319 models.

320

321 *4.2. Laboratory experiments*

322 The soil hydraulic properties estimated in the laboratory soil columns are summarized in
323 Table 3. As observed in synthetic homogenous soil (Fig. 4a), the decrease of RMSE with time
324 observed in the uniform loam soil is also present in the uniform laboratory loam (Fig. 5a). The
325 soil uniformity is also corroborated by the almost constant K_s and S values estimated along

the whole infiltration time. The *WFA* calculated for the loam and clay loam soils (Table 3) were close to the 4.2 - 4.4 cm thickness of the wetted soil bulb measured in both soils at the end of the experiment.

A different behavior was observed in the stratified soil columns. The minimum RMSE found with the SIA method indicated a change of soil layer at time t_o, corresponding to the minimum RMSE value (Fig. 5b and c). The smaller t_o observed in the sand+clay loam (S+CL) column (Fig. 5c) may be related to the significant higher K_s and S of the sand (Table 3), which accelerated the infiltration that reaches the lower layer in less time. However, although the two columns presented an absolute minimum of the RMSE, the K_s behavior after time t_o was different in the two experiments. The large variability of K_s around its optimal value observed in loam soil+clay loam (L+CL) column (Fig. 5b) indicates that the model cannot fit the experimental curve, probably due to the extra concavity observed at large times. The change of soil layer, however, was more evident in the S+CL profile (Fig. 5c), where much contrasted K_s and S values were obtained (Table 3). In this case, the smaller K_s and S of the clay loam soil generated an infiltration curve with a shift in its slope and shape, and with a significant decrease in K_s with time.

Overall, the similarity of K_s and S estimates between the homogeneous loam and sand columns, on one hand, and the layered profiles, on the other, (Table 3), indicates that the method was robust and pointed at accurate estimates of the hydraulic properties in all the cases. Overall, the thickness of the upper soil layer predicted from *WFA* values was close to their actual value (Table 3). As observed in the synthetic soils, these results indicate the SIA method allowed estimating the thickness of the upper soil layer. The robust relationship between K_s and S estimates obtained with QEI and 4T models ($y = 1.013x + 0.022$; R^2 =

349 0.9091; $p < 0.0001$), is in line with previous results and indicates that 4T model is accurate to
350 estimate the soil hydraulic properties.

351

352 *4.3. Field measurements*

353 Overall, the field soils presented a sandy loam texture, high amount of gypsum (73%) and
354 low organic matter content (1.66%). A great variability of types and shapes of infiltration
355 curves was observed from field experiments (Fig. 6). Given the different types of cumulative
356 infiltration curves described by Angulo-Jaramillo et al. (2019), four main types were analyzed:
357 (i) a regular (Fig. 7a), (ii) extra-concavity (Fig. 7b), (iii) double-slope infiltration curve
358 previously checked that it was affected by water repellency phenomena (Fig. 7c), and (iv)
359 infiltration showing some irregularities at early times (Fig. 7d).

360 In the first case (M1M2R2, Fig. 7a), a standard curve corresponding to a homogeneous soil,
361 where the RMSE decreased along all the experiment (> 600 s), with its corresponding
362 estimates reported in Table 4. Other indicators corroborating the homogeneity of this soil were
363 the stability of S and K_s estimates and the almost constant time for the contact sand layer, t_{sand}.
364 These results suggest that the soil profile at the place of this infiltration curve was
365 homogeneous. The thickness of the corresponding soil layer was 4.3 cm (Table 4).

366 In the second example (M1L5R1, Fig. 7b), although a preliminary visual analysis might
367 suggest a behavior similar to the previous curve, the sequential analysis evidenced the
368 existence of a non-uniform soil profile within the measured infiltration time. The decreasing
369 behavior of the infiltration rate, which corresponds to a kind of extra-concavity defined by
370 Angulo-Jaramillo et al. (2019), was similar to that observed in the L1cm+Si synthetic soil
371 (Fig. 4b) and also in the stratified laboratory soil columns (Fig. 5b and c). The minimum

RMSE was located around 170 s (t_o), time from which the RMSE increased to the end of the infiltration. Other indicator of the existence of a layered profile was the decrease of K_s and the large variation of t_{sand} from t_o. This large t_{sand} variation is due to the model had to adapt the t_{sand} value to find the best fitting for the heterogeneous profile. On the other hand, the decrease of K_s over time would indicate that the profile presented a less permeable deeper layer (Di Prima et al., 2018). Although less evident, these changes were also manifested in *S*, whose values kept almost constant until t_o (170 s) before increasing. In this case, the thickness of the top soil layer was 1.4 cm (Table 4). Thus, the sequential analysis of the infiltration curve suggested the existence of a heterogeneous profile with a less permeable deeper layer.

A different behavior was depicted in Figure 7c (M1L3R1), where an inflection point was observed around 150 s. This behavior was due to water repellence phenomenon (Moret-Fernández et al., 2019), as previously experimentally checked with the water drop penetration time (WDPT) test (Watson and Letey, 1970). When water infiltrates into hydrophobic soils, the water advance during the early phase of wetting is impeded owing to hydrophobic surface films on soil particles (Jarvis et al., 2008). However, once the hydrophobic layer is overcome (t_o), the infiltration rise promoted a significant increase of RMSE and K_s, and a decrease of *S*. An important increase of t_{sand} was also observed just after the inflection point. Although water repellency, and hence the inflection point, can be visually detected (Angulo-Jaramillo et al., 2019), the minimum RMSE located with the SIA procedure allowed a more objective determination of t_o and, hence, more accurate estimates of *S* and K_s. The average thickness of the top soil layer measured from *WFA* was around 1.2 cm (Table 4).

In the last example (M1M2R1, Fig. 7d), a curve with an unclear behavior is presented. In this case, if the determination of t_o is only based on the absolute RMSE minimum, a t_o around 210 s was obtained (discontinuous vertical line). However, a more detailed analysis indicated that after the absolute RMSE minimum there is another local minimum that coincides with

more stable t_{sand}, S and K_s values. Since the dispersion of all variables with time was relatively small, in this case we would suggest omitting the initial times (grey points in Fig. 5d) and analyze the remaining infiltration section. In this case, t_o increased up to 680 s (Table 4) and the corresponding *WFA* was about 3.4 cm. All these examples demonstrated that the SIA method can be applied to real experimental data and should be considered when accurate estimates of hydraulic properties are required.

Overall, similar S, K_s, t_o, α, n and *WFA* values were obtained with both QEI and 4T models (Table 4). The robust relationships between the hydraulic parameters estimated with both models (Table 5) indicates that hydraulic properties could be indistinctly estimated with QEI or 4T models. The small differences between both models could be explained by the different time increment employed to remove the effect of the contact sand layer (Latorre et al., 2015): 0.5 vs. 0.1 s for QEI and 4T, respectively. Preliminary analyses of synthetic soils with sand layer using the same time increment (0.1 s) confirmed not significant differences between QEI and 4T only attributed to the different employed optimization algorithms. The larger time interval used in QEI is the result of a compromise between computation time and accuracy. That is to say, shorted time intervals would result in excessively long calculation times. However, the simpler and faster analysis of the 4T model allowed reducing this time interval, which might result in better estimates of the hydraulic properties. These results suggest that the 4T expansion is a robust alternative to estimate the soil hydraulic properties from the inverse analysis of a cumulative infiltration curve within a large range of infiltration times.

The S and K_s estimated from the measured infiltration curves ranged between 0.07 to 0.60 mm $s^{-0.5}$ and 1.8 10^{-3} to 3.72 10^{-2} mm s^{-1}, respectively. Over the 20 experimental infiltrations, only 3 measurements presented a t_o equal to the total measured infiltration time (≈600 s); 25 % of the analyzed curves presented t_o > 400 s and 200 < t_o < 400, respectively, and 50% a t_o < 200 s. These results would indicate that for the most cases the hydraulic properties were

estimated from short to medium infiltration times. For the 70% of the studied soils, the estimated upper soil layer was thinner than 2 cm, and only three soils presented a uniform upper layer wider than 4 cm. These results suggest that, overall, the analyzed soils presented a thin upper layer, which could probably correspond with the soil surface crust.

5. CONCLUSIONS

This work presents a procedure to analyze the infiltration curves measured on layered soil profiles. This new method, referred as SIA, Sequential Infiltration Analysis, consists of analyzing infiltration curves at increasing time intervals, and calculating the corresponding K_s, S and the RMSE characterizing the quality of the fit. To this end, both QEI and 4T models were employed. A procedure to estimate the wetting front advance (*WFA*) or the thickness of the upper uniform soil layer from the infiltration analysis was also presented. The procedure, which was applied on synthetic layered profiles and experimental soils, showed that erroneous estimates of K_s and S were obtained when the inverse analysis was applied to the whole infiltration curve obtained for heterogeneous profiles. This limitation, however, vanished using the SIA procedure, which allowed satisfactory estimates of t_o, K_s, S and the corresponding *WFA* for very different types of infiltration curves. However, because the SIA method sequentially analyzes the series of infiltrations, results only correspond to the upper soil layer, which can be considered homogeneous. This hypothesis implies a limitation of the method when the thickness of the upper layer is very thin. On the other hand, since the results also show that some of the properties of the deepest soil layers are also contained in the infiltration curve, it opens the possibility to advance in the method improvement to obtain

446 additional information of the total soil profile from the analysis of the complete infiltration
447 curve. In most experimental soils, only short to medium infiltration times could be analyzed,
448 and the thickness of the upper homogeneous soil layer ranged between 1 and 5 cm. In
449 conclusion, these results showed that great care must be taken when calculating the soil
450 hydraulic properties from the inversion of the measured infiltration curves, questioning the
451 possibility that anomalous curves cannot be analyzed accurately. On the other hand, although
452 similar results were obtained with both QEI and 4T models, the simpler and faster analysis
453 allowed by 4T suggests that this expansion can be a robust alternative to be implemented in
454 the SIA method for the estimation of the K_s and S of the top layer of layered soil profiles

455

456 **Acknowledgments**

457 This research was supported by the Ministerio de Economía, Industria y Competitividad,
458 project PROPAST (CGL2016-80783-R) and ASBIO (PGC2018-094332-B-100), the
459 International Emerging Action (IEA) (PICS08250), and in part supported by the European
460 Regional Development Fund (ERDF) and the Italian Ministry of Education, University and
461 Research (MIUR) through the "Programma Operativo Nazionale (PON) Ricerca e
462 Innovazione 2014-2020 (Linea 1 - Mobilità dei ricercatori, AIM1853149, CUP:
463 J54I18000120001). The authors are grateful to Área de Informática Científica of SGAI
464 (CSIC) for their technical support in the numerical analysis and to R. Gracia and M.J. Salvador
465 for technical help in several aspects of this study.

466

467 **References**

468 Angulo-Jaramillo, R., Bagarello, V., Di Prima, S., Gosset, A., Iovino, M., Lassabatere, L.
469 2019. Beerkan Estimation of Soil Transfer parameters (BEST) across soils and scales.
470 Journal of Hydrology 576, 239–261.

471 Angulo-Jaramillo, R., Vandervaere, J.P., Roulier, S., Thony, J.L., Gaudet, J.P., Vauclin, M.
472 2000. Field measurement of soil surface hydraulic properties by disc and ring
473 infiltrometers. A review and recent developments. Soil Tillage Research 55, 1–29.

474 Ankeny, M.D., Ahmed, M., Kaspar, T.C., Horton, R., 1991. Simple field method determining
475 unsaturated hydraulic conductivity. Soil Sci. Soc. Am. J. 55, 467– 470.

476 Bates, D. M., Watts, D. G. 1988 Nonlinear Regression Analysis and Its Applications, Wiley.

477 Bates, D. M., Chambers, J. M. 1992 Nonlinear models. Chapter 10 of Statistical Models in S
478 eds J. M. Chambers and T. J. Hastie, Wadsworth & Brooks/Cole.

479 Beatty, S.M., Smith, J.E., 2013. Dynamic soil water repellency and infiltration in postwildfire
480 soils. Geoderma 192, 160–172.

481 Carsel, R.F., Parrish, R.S., 1988. Developing joint probability distributions of soil water
482 retention characteristics. Water Resour. Res. 24, 755–769.

483 Di Prima, S., Concialdi, P., Lassabatere, L., Angulo-Jaramillo, R., Pirastru, M., Cerdà, A.,
484 Keesstra, S., 2018. Laboratory testing of Beerkan infiltration experiments for
485 assessing the role of soil sealing on water infiltration. CATENA 167, 373–384.

486 Fernandez-Galvez, J., Pollacco, J.A.P., Lassabatere, L., Angulo-Jaramillo, R., Carrick, S.
487 2019. A general Beerkan Estimation of Soil Transfer parameters method predicting
488 hydraulic parameters of any unimodal water retention and hydraulic conductivity

curves: Application to the Kosugi soil hydraulic model without using particle size distribution data. Advances in Water Resources 129, 118-130.

Grossman, R.B., Reinsch, T.G., 2002. Bulk density and linear extensibility. In: Dane, J.H., Topp, G.C. (Eds.), Methods of Soil Analysis. Part 4. SSSA Book Series No. 5. Soil Science Society of America, Madison, WI.

Fernández-Gálvez, J., Pollacco, J. A. P., Lassabatere, L., Angulo-Jaramillo, R. and Carrick, S. 2019. A general Beerkan Estimation of Soil Transfer parameters method predicting hydraulic parameters of any unimodal water retention and hydraulic conductivity curves: Application to the Kosugi soil hydraulic model without using particle size distribution data, Advances in Water Resources, 129, 118–130, doi:10.1016/j.advwatres.2019.05.005.

Haverkamp, R., Ross, P.J., Smettem, K.R.J., Parlange, J.Y., 1994. Three dimensional analysis of infiltration from the disc infiltrometer. Part 2. Physically based infiltration equation. Water Resour. Res. 2931–2935.

Heanes, D.L., 1984. Determination of total organic-C in soils by an improved chromicacid digestion and spectrophotometric procedure. Commun. Soil Sci. Plant Anal. 15, 1191–1213.

Horst, R., Romeijn, H.E. (Eds.), 2002. Handbook of Global Optimization, vol. 2.Springer Science & Business Media.

Iovino, M., Angulo-Jaramillo, R., Bagarello, V., Gerke, H.H., Jabro, J., Lassabatere, L., 2017. Thematic Issue on Soil Water Infiltration. Journal of Hydrology and Hydromechanics 65, 205–208. https://doi.org/10.1515/johh-2017-0036

511 Jarvis, N., Etana, A., Stagnitti, F., 2008. Water repellency, near-saturated infiltration and
512 preferential solute transport in a macroporous clay soil. Geoderma 143, 223–230.

513 Lassabatere, L., Di Prima, S., Angulo-Jaramillo, R., Keesstra, S., Salesa, D., 2019. Beerkan
514 multi-runs for characterizing water infiltration and spatial variability of soil hydraulic
515 properties across scales. Hydrol. Sci. J. 64, 165–178.

516 Lassabatere, L., Angulo-Jaramillo, R., Soria, J.M., Cuenca, R., Braud, I., Haverkamp, R.
517 2006. Beerkan estimation of soil transfer parameters though infiltration experiments –
518 BEST. Soil Sci. Soc. Am. J. 70, 521.532.

519 Lassabatere, L., Angulo-Jaramillo, R., Soria-Ugalde, J.M., Simunek, J., Haverkamp, R., 2009.
520 Numerical evaluation of a set of analytical infiltration equations. Water Resour. Res.
521 https://doi.org/10.1029/2009WR007941.

522 Lassabatere, L., Yilmaz, D., Peyrard, X., Peyneau, P.E., Lenoir, T., Šimůnek, J., Angulo-
523 Jaramillo, R., 2014. New analytical model for cumulative infiltration into dual-
524 permeability soils. Vadose Zone Journal 13, 1–15.
525 https://doi.org/10.2136/vzj2013.10.0181

526 Lassabatere, L., Angulo-Jaramillo, R., Goutaland, D., Letellier, L., Gaudet, J.P., Winiarski,
527 T., Delolme, C., 2010. Effect of the settlement of sediments on water infiltration in two
528 urban infiltration basins. Geoderma 156, 316–325.
529 https://doi.org/10.1016/j.geoderma.2010.02.031

530 Latorre, B., Peña, C., Lassabatere, L., Angulo-Jaramillo, R., Moret-Fernández, D., 2015.
531 Estimate of soil hydraulic properties from disc infiltrometer three-dimensional
532 infiltration curve. Numerical analysis and field application. J. Hydrol. 57, 1–12.

533 Latorre, B., Moret-Fernández, D., Lassabatere, L., Rahmati, M., López, M.V., Angulo-
534 Jaramillo, R., Sorando, R., Comín, F., Jiménez, J.J. 2018. Influence of the β parameter
535 of the Haverkamp model on the transient soil water infiltration curve. J. Hydrol. 564,
536 222–229.

537 More, J.J. 1978. The Levenberg-Marquardt algorithm: implementation and theory; in Lecture
538 Notes in Mathematics 630: Numerical Analysis, G.A. Watson (Ed.), Springer-Verlag:
539 Berlin, pp. 105-116.

540 Moret-Fernández, D., Latorre, B., Angulo-Martínez, M. 2017. Comparison of different
541 methods to estimate the soil sorptivity from an upward infiltration curve. Catena 155,
542 86–92.

543 Moret-Fernández, D., Latorre, B. 2017. Estimate of the soil water retention curve from the
544 sorptivity and β parameter calculated from an upward infiltration experiment. J. Hydrol.
545 544, 352–362

546 Moret-Fernández, D., Blanco, N., Martínez-Chueca, V., Bielsa, A. 2013. Malleable disc base
547 for direct infiltration measurements using the tension infiltrometry technique. Hydrol.
548 Proc. 27, 275, 283.

549 Moret-Fernández, D., Latorre, B., López, M.V., Pueyo, Y., Lassabatere, L., Angulo-Jaramilo,
550 R., Rahmati, M., Tormo, J., Nicolau, J.M. 2020. Three- and four-term approximate
551 expansions of Haverkamp formulation to estimate soil hydraulic properties from disc
552 infiltrometer measurements. Hydrological Processes, DOI: 10.1002/hyp.13966.

553 Moret-Fernández, D., Latorre, B., Giner, M.L., Ramos, , J, Alados, C.L., Castellano, C.,
554 López, M.V., Jimenez, J.J. , Pueyo, Y. 2019. Estimation of the soil hydraulic properties

555 from the transient infiltration curve measured on soils affected by water repellency.
556 Catena 178, 298–306

557 Mualem, Y. 1976. A new model for predicting the hydraulic conductivity of unsaturated
558 porous media. Water Resour. Res. https://doi.org/10.1029/WR012i003p00513.

559 Navas, A. 1991. The pattern of gypsum transport in the Ebro river network. Catena 18, 45-49.

560 Parlange, J.Y. 1975. On solving the flow equation in unsaturated flow by optimization:
561 horizontal infiltration. Soil Sci. Soc. Am. J. 39, 415–418.

562 Perroux, K.M., White, I., 1988. Designs for disc permeameters. Soil Sci. Soc. Am. J. 52,
563 1205–Philip, J.R., 1957. The theory of infiltration: 4. Sorptivity and algebraic
564 infiltration equations. Soil Sci. 84, 257–264.1215.

565 Porta J., Lopez-Acebedo M., Rodriguez R. 1986. Tecnicas y experimentos en edafologıa. Dep.
566 de Cien-cias del Suelo-ETSIA. Lerida, Spain.

567 Rahmati, M., Latorre, B., Lassabatere, L., Angulo-Jaramillo, R., Moret-Fernández, D. 2019.
568 The relevance of Philip theory to Haverkamp quasi-exact implicit analytical formulation
569 and its uses to predict soil hydraulic properties. Journal of Hydrology 570, 816–826.

570 Šimunek, J., Šejna, M., van Genuchten, M.-Th., 1999. The HYDRUS-2D Software Package
571 for Simulating the Two-dimensional Movement of Water, Heat, and Multiple Solutes in
572 Variably-saturated Media. Version 2.0. U.S. Salinity laboratory, Agricultural Research
573 Service, USDA, Riverside, California.

574 Simunek, J., van Genuchten, M.T., 1996. Estimating unsaturated soil hydraulic properties
575 from tension disc infiltrometer data by numerical inversion. Water Resour. Res. 32,
576 2683–2696.

577 Smettem, K., Parlange, J., Ross, P. and Haverkamp, R.: Three-dimensional analysis of
578 infiltration from the disc infiltrometer: 1. A capillary-based theory, Water Resources
579 Research, 30(11), 2925–2929.

580 van Genuchten, M.T., 1980. A closed form equation for predicting the hydraulic conductivity
581 of unsaturated soils. Soil Sci. Soc. Am. J. 44, 892–898.

582 Vandervaere, J.-P., Vauclin, M., Elrick, D.E., 2000. Transient flow from tension infiltrometers
583 I. The two-parameter equation. Soil Sci. Soc. Am. J. 64 (4), 1263–1272.

584 Watson, C.L., Letey, J., 1970. Indices for characterizing soil-water repellency based upon
585 contact angle-surface tension relationships. Soil Sci. Soc. Am. J. 34, 841–844.

586

587 **Figures captions**

588

589 **Figure 1**. Diagram of the considered cumulative infiltration equations, QEI and its
590 corresponding 4T approximation.

591

592 **Figure 2**. Schema of the synthetic soil experiments simulated with HYDRUS-3D.

593

594 **Figure 3**. Description of the conducted laboratory experiments using a tension disc
595 infiltrometer.

596

597 **Figure 4**. (a) Cumulative infiltration curves simulated on a homogeneous synthetic loam soil
598 (L) and 1 and 3cm loam layer followed by a sandy loam (SL) and silt (Si) layers, and
599 the corresponding temporal evolution of the (b) RMSE, (c) soil sorptivity, S, and (c)
600 saturated hydraulic conductivity, K_s. Vertical lines denote the optimal time, t_o,
601 corresponding to the minimum RMSE, and horizontal lines in (c) and (d) indicate the
602 theoretical S and K_s values.

603

604 **Figure 5**. Measured (Exp) and optimized (Opt) cumulative infiltration curves and temporal
605 evolution of the RMSE, soil sorptivity, S, and saturated hydraulic conductivity, K
606 estimated from (a) homogeneous loam soil, (b) 3 cm thickness loam soil followed by
607 clay loam and (c) 3 cm thickness sand followed by clay loam columns. Vertical lines

608 denote the optimal time, t_o, for the corresponding simulations and horizontal green and
609 blue lines indicate the optimal S and K_s values, respectively.

610

611 **Figure 6**. Cumulative infiltration curves measured in field conditions.

612

613 **Figure 7**. Measured (Exp) and optimized (Opt) cumulative infiltration curves, and temporal
614 evolution of the contact sand layer, t_{sand}, RMSE, soil sorptivity, S, saturated hydraulic
615 conductivity, K_s, corresponding to the (a) M1M2R2, (b) M1L5R1, (c) M1L3R1 and
616 (d) M1M2R1 sampling points. Vertical lines denote the optimal time, t_o, of the
617 simulations and horizontal blue and green lines are the corresponding optimal K_s and
618 S values.

619

620

621 **Table 1.** Initial, θ_i, residual, θ_r, and final,
622 θ_s, soil volumetric water contents,
623 sorptivity, S (Eq. 8), saturated hydraulic
624 conductivity, K_s, α and n parameters of van
625 Genuchten (1980) model of synthetic
626 sandyloam, loam and silt soils.

Soil	θ_s $cm^3\ cm^{-3}$	θ_i, θ_r, $cm^3\ cm^{-3}$	α mm^{-3}	n	K_s $mm\ s^{-1}$	S^* $mm\ s^{-0.5}$
Sandyloam	0.41	0.065	0.75	1.89	$1.23\ 10^{-2}$	0.635
Loam	0.43	0.078	0.36	1.56	$2.88\ 10^{-3}$	0.367
Silt	0.46	0.034	0.16	1.37	$6.94\ 10^{-4}$	0.238

627 *Moret-Fernández et al. (2017)

628

Table 2. Soil sorptivity, *S*, saturated hydraulic conductivity, K_s, optimal time for the best optimization, t_o, and wetting front advance, *WFA*, estimated with QEI and 4T expansion for the synthetic soils of Table 1.

Soil	*QEI*				*4T*			
	S	K_s	t_o	*WFA*	*S*	K_s	t_o	*WFA*
	mm $s^{-0.5}$	mm s^{-1}	s	cm	mm $s^{-0.5}$	mm s^{-1}	s	Cm
L	0.369	0.0023	1800	4.79	0.370	0.0024	1800	4.82
L_{1cm} + SL	0.340	0.0035	100	0.99	0.366	0.0034	100	1.06
L_{2cm} + SL	0.370	0.0023	250	1.70	0.370	0.0024	250	1.70
L_{3cm} + SL	0.370	0.0023	600	2.68	0.370	0.0023	650	2.80
L_{1cm} + Si	0.370	0.0033	100	1.07	0.364	0.0033	150	1.30
L_{2cm} + Si	0.367	0.0026	300	1.86	0.368	0.0025	350	2.02
L_{3cm} + Si	0.368	0.0023	600	2.67	0.369	0.0023	700	2.89

629

630

Table 3. Measured initial/residual (θ_i / θ_r) and saturated volumetric water content (θ_s) total infiltration time (t_t) and optimum infiltration time (t_o), sorptivity (S) and saturated hydraulic conductivity (K_s), and estimated wetting front advance (*WFA)* values calculated with QEI and 4T model.

				QEI				*4T*			
	θ_i / θ_r	θ_s	t_{max}	t_o	S	K_s	*WFA*	t_o	S	K_s	*WFA*
	$cm^3\ cm^{-3}$		s		$mm\ s^{-0.5}$	$mm\ s^{-1}$	cm	s	$mm\ s^{-0.5}$	$mm\ s^{-1}$	cm
Sand	0.03	0.390	15	-	-	-	-	9	1.9	$8.6\ 10^{-1}$	2.69
Loam	0.03	0.417	910	866	0.51	$1.7\ 10^{-3}$	3.98	881	0.52	$6.4\ 10^{-4}$	4.02
Clay loam	0.02	0.470	876	854	0.52	$9.6\ 10^{-4}$	3.42	839	0.53	$1.6\ 10^{-3}$	3.48
3 cm loam + clay loam	0.03	0.417	560	415	0.52	$3.5\ 10^{-3}$	2.83	410	0.53	$3.\ 9\ 10^{-4}$	2.78
3 cm sand + clay loam	0.03	0.390	1335	-	-	-	3.11	9	1.05	$9.6\ 10^{-1}$	3.11

631

632

Table 3. Measured initial/residual (θ_r / θ_r) and saturated volumetric water content (θ_s) total infiltration time (t_t) and optimum infiltration time (t_o), sorptivity (S) and saturated hydraulic conductivity (K_s) estimated with QEI and 4T models from disc infiltrometer measurements.

	θ_r / θ_r	θ_s	t_t	t_o		S		K_s		*WFA*	
				QEI	4T	QEI	4T	QEI	4T	QEI	4T
	$cm^3\ cm^{-3}$			s		$mm\ s^{-0.5}$		$mm\ s^{-1}$		cm	
M1L1R1	0.03	0.42	960	148	148	0.25	0.25	$1.80\ 10^{-03}$	$1.58\ 10^{-03}$	0.62	0.62
M1L1R2	0.04	0.51	899	260	325	0.07	0.09	$1.00\ 10^{-02}$	$1.06\ 10^{-02}$	0.67	0.88
M1L2R1	0.03	0.38	837	142	100	0.26	0.27	$2.57\ 10^{-03}$	$2.71\ 10^{-03}$	0.92	0.79
M1L2R2	0.02	0.41	779	217	297	0.25	0.25	$1.17\ 10^{-02}$	$1.15\ 10^{-02}$	1.20	1.48
M1L3R1	0.02	0.50	743	137	156	0.36	0.37	$1.07\ 10^{-02}$	$8.92\ 10^{-03}$	0.98	1.05
M1L3R2	0.04	0.51	898	145	145	0.04	0.03	$5.50\ 10^{-03}$	$5.38\ 10^{-03}$	0.20	0.20
M1L4R1	0.04	0.48	866	316	287	0.28	0.27	$2.29\ 10^{-02}$	$2.30\ 10^{-02}$	2.02	1.85
M1L4R2	0.03	0.51	857	357	266	0.13	0.11	$1.20\ 10^{-02}$	$1.17\ 10^{-02}$	1.05	0.76
M1L5R1	0.03	0.45	720	208	172	0.31	0.31	$1.19\ 10^{-02}$	$1.25\ 10^{-02}$	1.28	1.14
M1L5R2	0.02	0.55	648	165	149	0.24	0.24	$1.55\ 10^{-02}$	$1.53\ 10^{-02}$	0.79	0.73
M1M1R1	0.04	0.42	842	184	163	0.19	0.20	$1.07\ 10^{-02}$	$9.14\ 10^{-03}$	0.89	0.83
M1M1R2	0.02	0.48	597	548	593	0.52	0.52	$2.95\ 10^{-02}$	$2.89\ 10^{-02}$	4.50	4.74
M1M2R1	0.04	0.50	907	644	708	0.41	0.41	$1.33\ 10^{-02}$	$1.38\ 10^{-02}$	3.07	3.30
M1M2R2	0.04	0.41	727	682	663	0.42	0.42	$1.38\ 10^{-02}$	$1.39\ 10^{-02}$	4.05	3.97
M1M3R1	0.04	0.47	774	139	139	0.34	0.38	$2.95\ 10^{-02}$	$2.50\ 10^{-02}$	1.40	1.40
M1M3R2	0.02	0.46	837	309	309	0.44	0.45	$9.44\ 10^{-03}$	$6.57\ 10^{-03}$	1.99	1.97
M1M4R1	0.03	0.43	777	178	100	0.14	0.14	$4.79\ 10^{-03}$	$6.55\ 10^{-03}$	0.55	0.40
M1M4R2	0.02	0.51	582	507	522	0.59	0.60	$2.29\ 10^{-02}$	$2.24\ 10^{-02}$	3.72	3.78
M1M5R1	0.04	0.48	751	175	194	0.17	0.18	$2.29\ 10^{-02}$	$2.19\ 10^{-02}$	1.09	1.17
M1M5R2	0.03	0.47	826	141	100	0.36	0.33	$3.31\ 10^{-02}$	$3.72\ 10^{-02}$	1.47	1.14

633

634

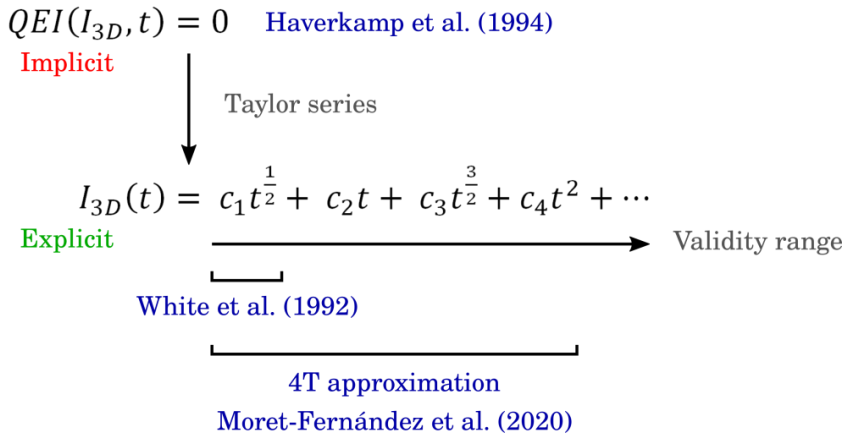

Figure 1.

635

636

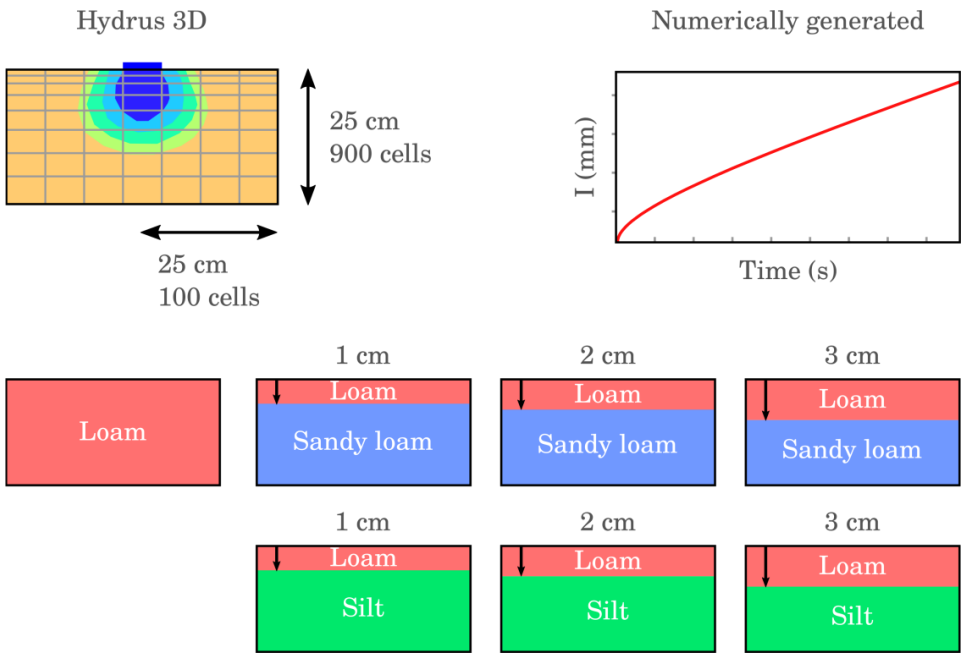

Figure 2.

637

638

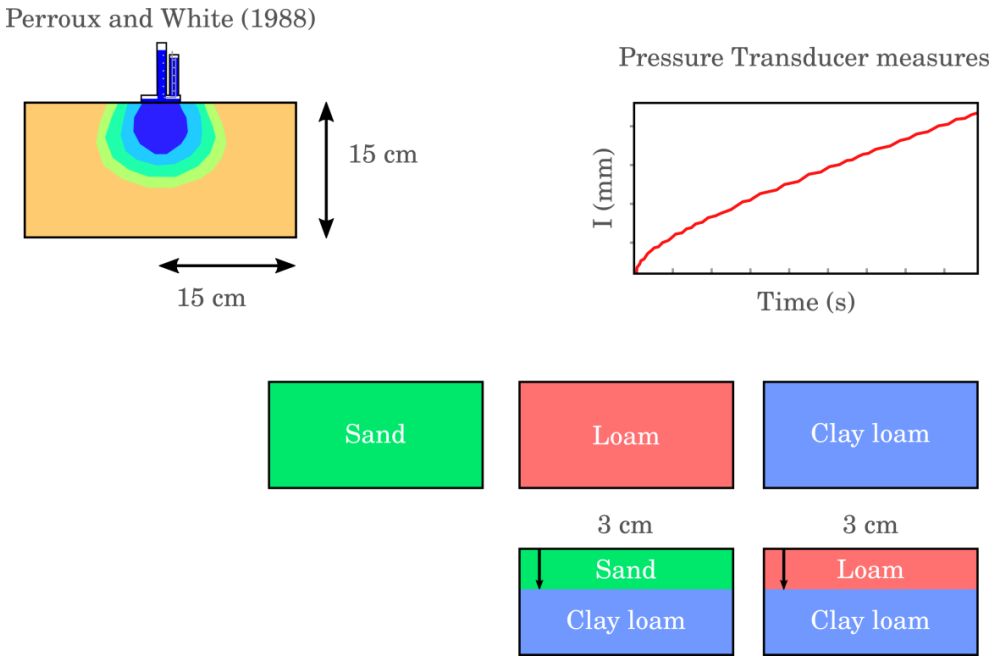

Figure 3.

639

640

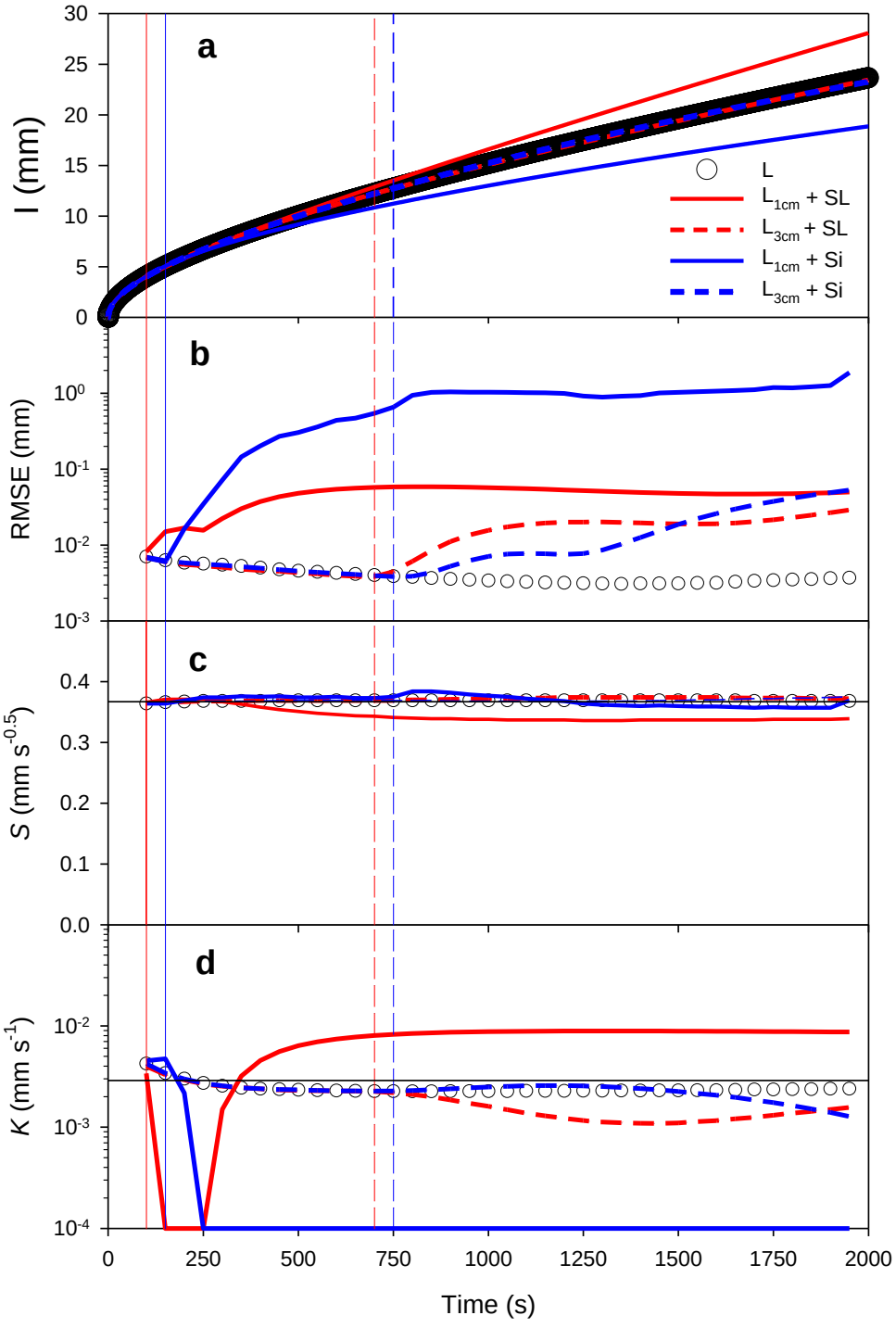

Figure 4.

641

642

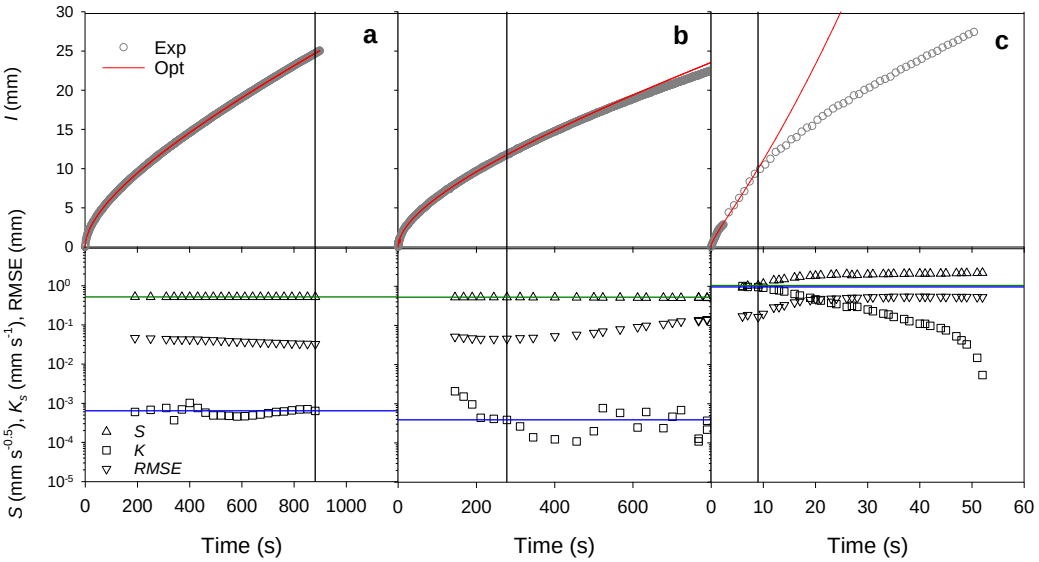

Figure 5.

643

644

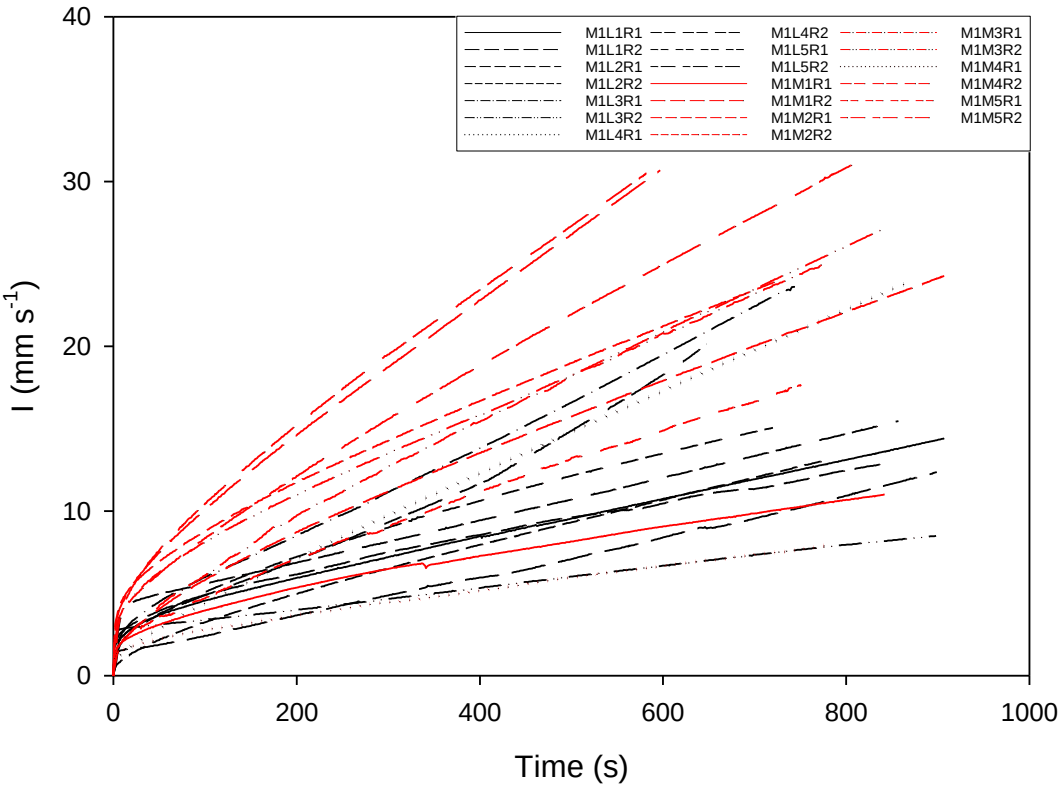

Figure 3.

645

646

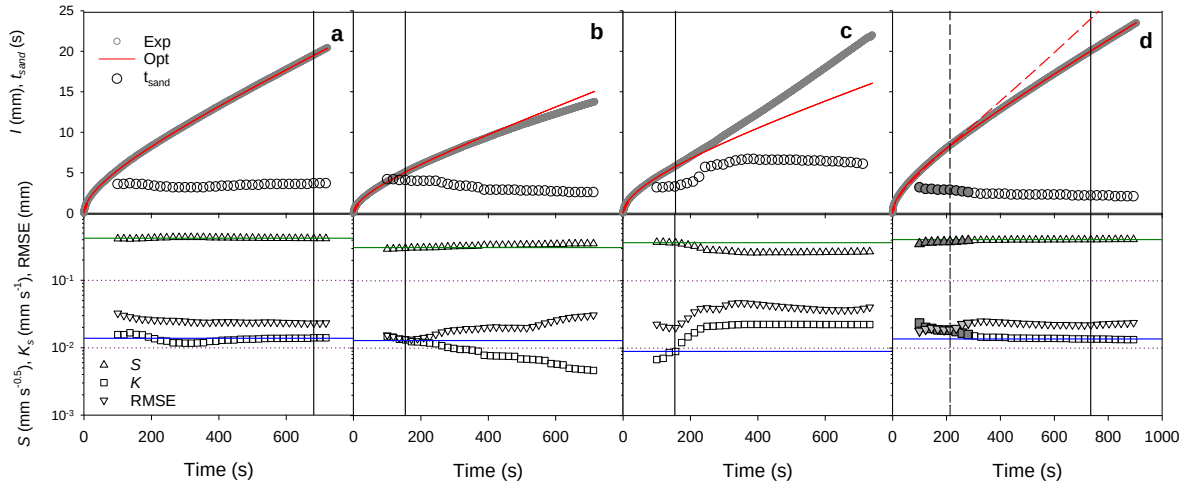

Figure 7.

647

648